Geostatistical AVA seismic inversion for reservoir characterisation of the Pozo D-129 Formation: A case study in San Jorge Basin, Argentina

Cecilia Zarpellón[1]*, Angie Padrón[1], Manuel Arijón[1], Antonio Ornés[2] and Paola Fonseca[2]

Abstract
A comprehensive seismic reservoir characterisation study was conducted in a gas field in Argentina, utilising geostatistical AVA seismic inversion to generate input for reliable static and dynamic model simulation. The study encompassed a range of disciplines, including petrophysics, rock physics modelling and geostatistical AVA seismic inversion, followed by effective porosity co-simulation.
The key advantage of the geostatistical inversion method lies in its ability to integrate all available data, i.e. wells, seismic, and geological knowledge, resulting in outcomes that honour all input and produce reliable results.
A notable aspect of this study was the use of 3D prior probabilities models for geostatistical inversion which proved to be crucial for better characterisation of litho-facies across the area, outperforming the 1D approach.
The results of the geostatistical inversion, combined with the conceptual depositional model and previous seismic attributes study, showed significant consistency, increasing confidence in the outcomes of the geostatistical inversion.
The results of this study will be used to build static models of the field, enabling estimation of the in-place gas volume and its associated uncertainty. These models will also serve as input for dynamic simulations for the future development of this field.

Introduction
A comprehensive seismic reservoir characterisation study was conducted in a gas field in Argentina, utilising geostatistical AVA seismic inversion to generate input for reliable static and dynamic model simulation. The study encompassed a range of disciplines, including petrophysics, rock physics modelling and geostatistical AVA seismic inversion, followed by effective porosity co-simulation. The outcome of this effort was a set of 20 equally probable realisations, generated within a 300 ms vertical time window, covering an area of approximately 180 km².

This study focused on the productive reservoirs in the upper interval of the Pozo D-129 Formation in the Chulengo field which was discovered in 2020 through the drilling of an exploratory well with an initial production of 275,000 m³/day of gas. To date,

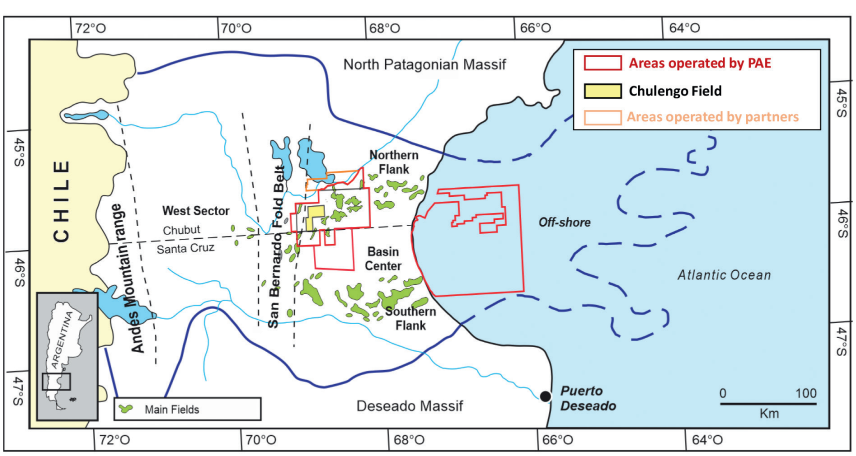

Figure 1 Location map showing the area of study: Chulengo field, Cerro Dragón area, Golfo San Jorge Basin, Argentina.

[1] Pan American Energy | [2] Viridien
* Corresponding author, E-mail: czarpellon@pan-energy.com
DOI: 10.3997/1365-2397.fb2025041

a total of five wells have been drilled, with a cumulative gas production of 415,174,000 m³ from 945,000,000 m³ of original gas in place (OGIP) (Canocini et al. 2023). This concession, operated by Pan American Energy (PAE) with a 100 % interest, is located in the Cerro Dragón area of the Golfo San Jorge Basin in the Chubut province of Argentina (Figure 1).

The Golfo San Jorge Basin is an intracratonic basin whose main axis has a predominantly west-east direction. It is limited to the north by the North Patagonian Massif, to the south by the Deseado Massif, to the west by the Andes Mountain range and to the east along the continental margin of the Atlantic Ocean (Figure 1) (Cohen et al., 2022).

A simplified stratigraphic column of the study area is shown in Figure 2. The Pozo D-129 Formation serves as both the primary source rock in this sedimentary basin and the reservoir rock of this study. Specifically, the target reservoirs are situated within the upper section of the Pozo D-129 Formation, as highlighted in Figure 2. These reservoirs consist of tuffaceous sandstones deposited by the vertical aggradation of gravitational processes that transported sediments from the lake platform to the foot of the slope thus forming lake fans during the Early Cretaceous period (López Angriman et al. 2014). The conceptual depositional model of the upper section of the Pozo D-129 Formation is depicted in Figure 3, where the Koro area is associated with the

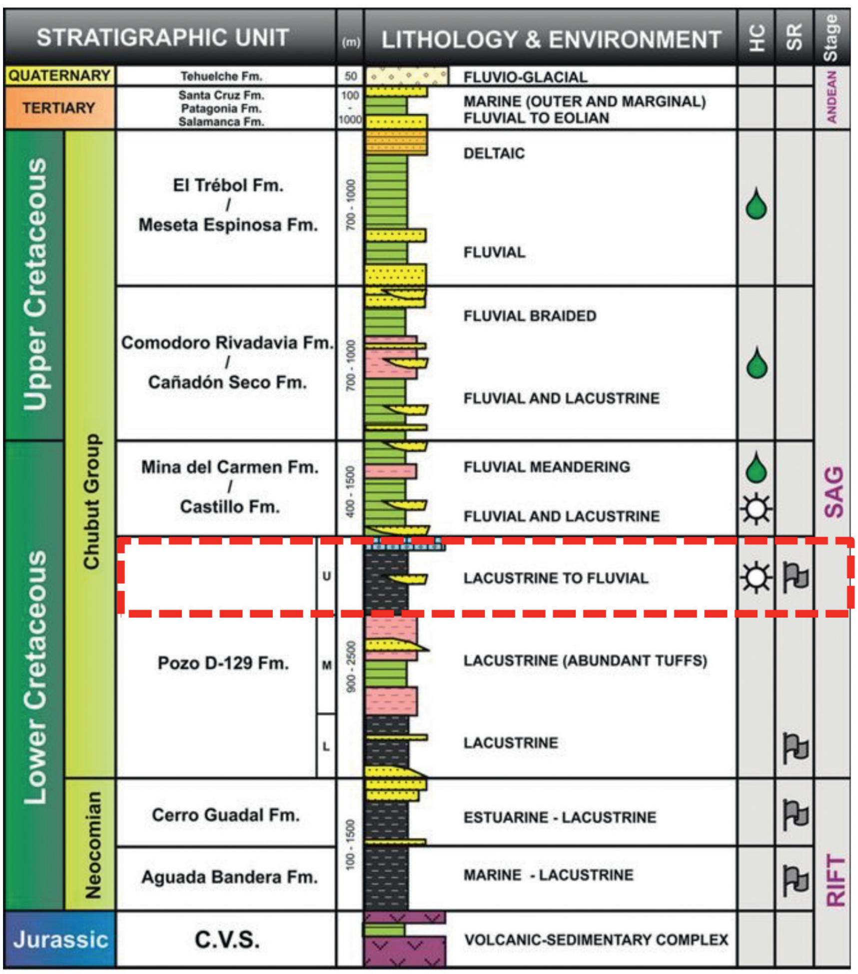

Figure 2 Stratigraphic column of the Cerro Dragón area. The target reservoirs are located within the upper section of the Pozo D-129 Formation (red rectangle).

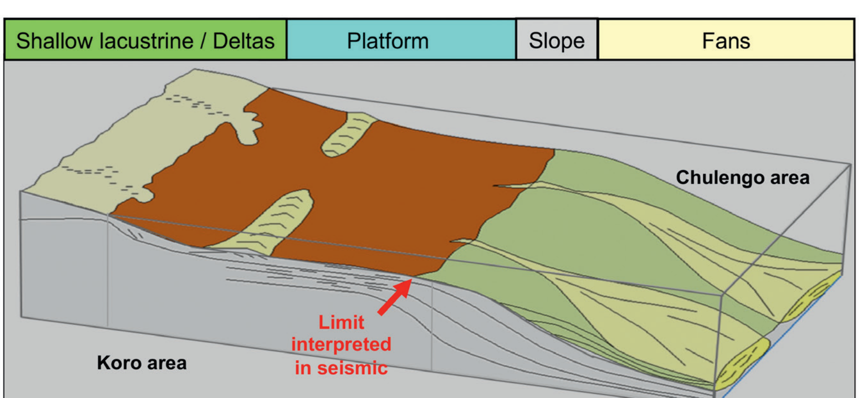

Figure 3 Conceptual depositional model of the upper section of the Pozo D-129 Formation, (modified after Brown and Fisher, 1977).

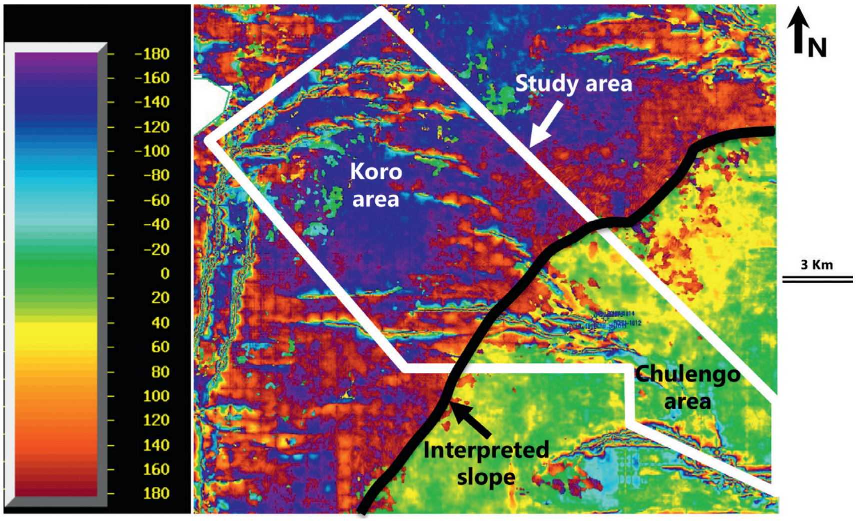

Figure 4 Instantaneous phase attribute map for the upper section of the Pozo D-129 Formation. The white polygon shows the study area, and the black line depicts the interpreted slope line.

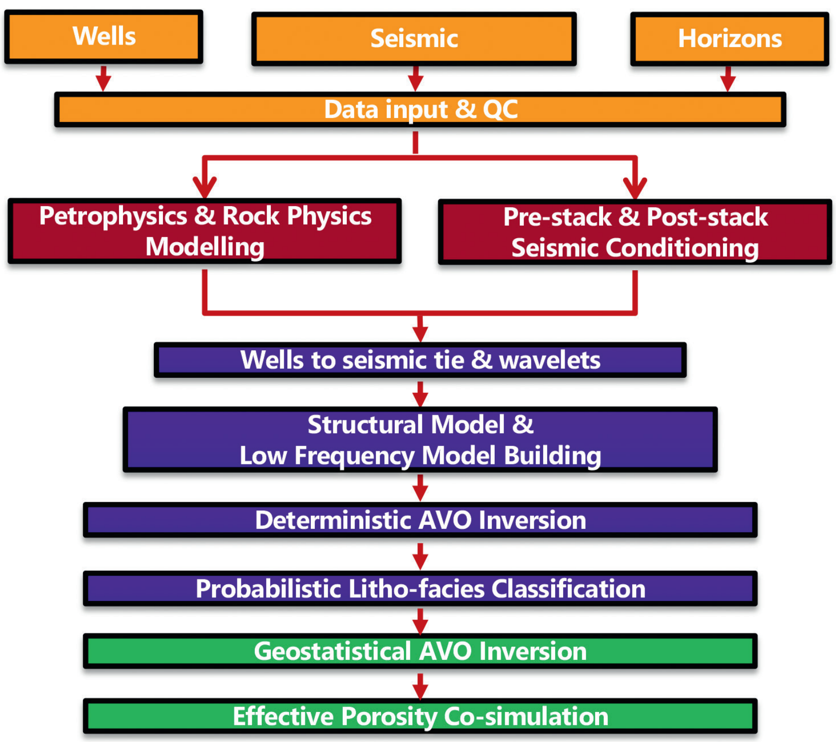

Figure 5 General workflow for the present study.

lake platform, the Chulengo area with lake fans and the slope representing the limit between the two areas.

The slope line, schematically represented in the conceptual depositional model (Figure 3), can reliably be interpreted using seismic attributes such as the instantaneous phase (Figure 4). In Figure 4, the white polygon shows the study area, and the black line depicts the interpreted slope line that clearly delimits zones with contrasting phases: the Koro area to the north-west of the slope line and the Chulengo area to the south-east of the line (Zarpellón, 2010).

The instantaneous phase map shown in Figure 4 suggests that this attribute is capable of differentiating depositional environments in the Pozo D-129 formation, showing instantaneous phase of around +/-180 degrees for platform deposits (Koro area) and around zero degrees for fan deposits (Chulengo area).

Methods

The scope of work included petrophysics, rock physics modelling and generation of litho-facies probability and elastic property volumes through geostatistical AVA seismic inversion. This was followed by computation of effective porosity volumes through co-simulation. The general workflow is summarised in Figure 5.

As the first stage of this study, petrophysics and rock physics modelling was conducted with ten wells. Five of these wells were in the Chulengo area, two in the Koro area and the other three wells were near the study area. First, a comprehensive log revision was performed which included editing and conditioning where required. Rock-physics modelled well logs were used later for deterministic and geostatistical inversions.

Integrated multi-disciplinary teams from Pan American Energy (PAE) and Viridien worked interactively to produce a petro-

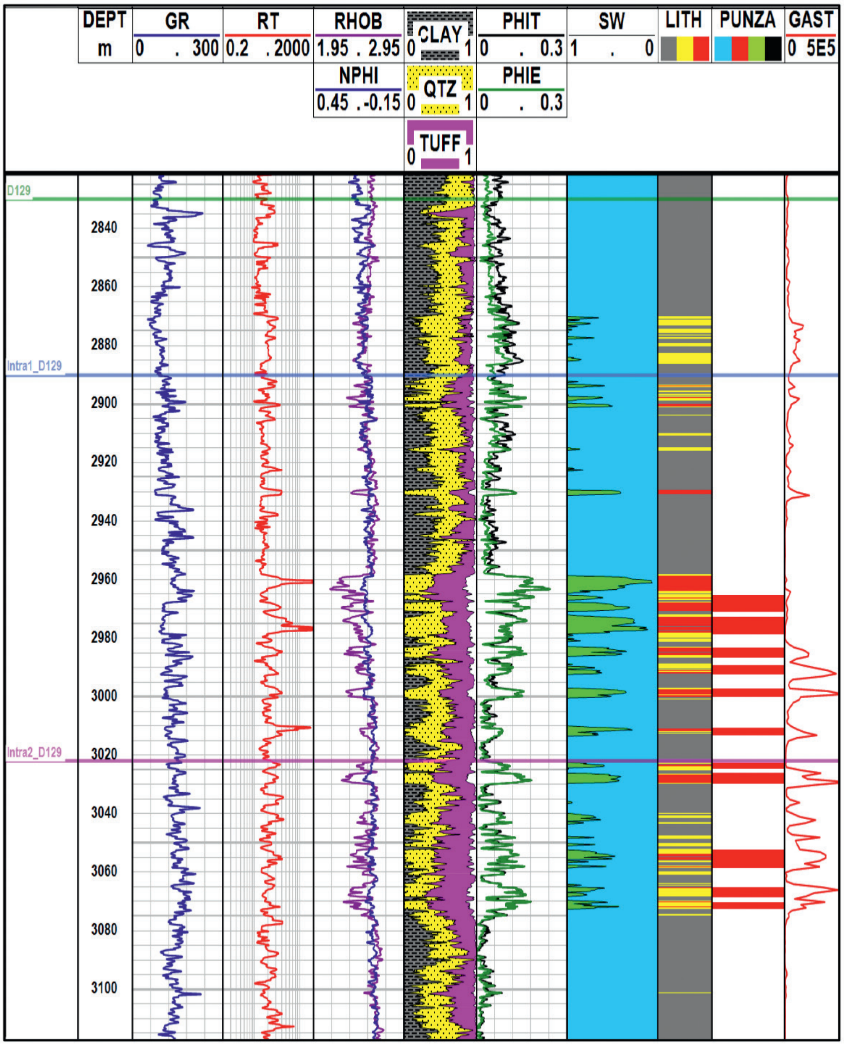

Figure 6 Petrophysical interpretation in one well of the Chulengo area.

physical and rock physics model that characterises the rock in terms of reservoir properties and elastic response simultaneously.

The petrophysical interpretation included clay, quartz and tuff volumes, effective and total porosity as well as water saturation. These results were calibrated using additional information, such as rotary side-wall core, magnetic resonance, tested intervals, and total gas curves. The rotary side-wall core data came from a well in the Chulengo area. The magnetic resonance interpretation was available in six wells in total, three of which were in the Chulengo area, two in the Koro area and one well near the study area. Furthermore, the water saturation curve was calibrated with tested intervals and a curve of total gas provided for all wells.

The complex mineral composition was generated from the response of several logs considering a multi-mineral approach which applies inverse statistical methods to a matrix containing curve responses and uncertainty values for formation constituents.

Porosities were calculated from the density log and weighted matrix density. Water saturation was estimated using Archie's model with the estimated effective porosity, a brine salinity of 9862 ppm of NaCl @ 91°C, a cementation exponent (m) of 2, a saturation exponent (n) of 2.1 and a tortuosity factor (a) of 1. Effective porosity was calculated by using the total porosity and shale volume, as PHIE = PHIT *(1-VSH).

Lithofacies	Cut-offs
Pay	PHIE >8% and SW <65%
Reservoir	PHIE >8%
Non Reservoir	PHIE <8%

Table 1 Definition of lithofacies based on their cut-offs.

Building on the results of the petrophysical evaluation, three lithofacies were determined based on effective porosity (PHIE) and water saturation (SW) cut-off, as shown in Table 1.

The results of petrophysical analysis in the upper interval of the Pozo D-129 Formation in one well of the Chulengo area are shown in Figure 6.

The overall good agreement observed between the pay litho-facies, tested intervals and total gas curves (Figure 6) suggested that the petrophysical interpretation was robust for the Pozo D-129 Formation.

A rock physics model provides the link between a rock's petrophysical and elastic properties. A grain-supported rock physics model for consolidated sand was used to model elastic logs. The main inputs for the model are fluid and mineral properties, petrophysical properties, such as porosity and water saturation, and the theoretical values for shear modulus, compressional

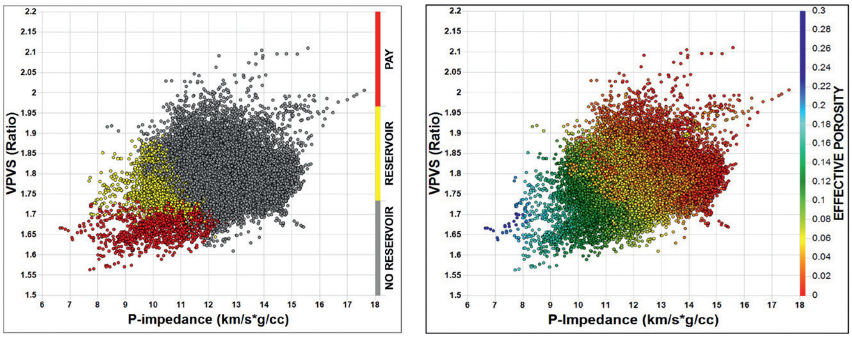

Figure 7 Modelled elastic cross plots with all ten wells in the Pozo D-129 Formation, colour-coded based on litho-facies (left) and effective porosity (right).

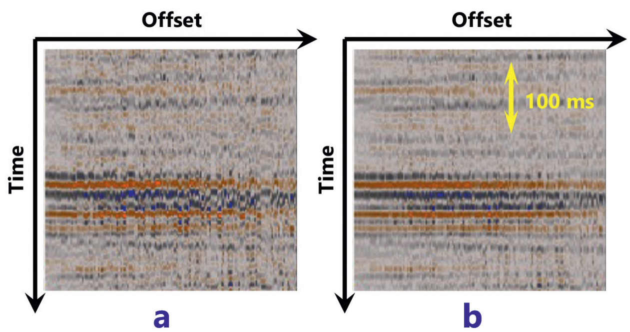

Figure 8 Pre-stack CDP gather before (a) and after (b) conditioning in the time window of interest.

modulus, and density for each mineral. Measured elastic logs (density, P-sonic and S-sonic) of good quality were used as a reference to calibrate the model.

Modelled P-impedance and Vp/Vs logs coloured by lithofacies (left) and effective porosity (right) are shown in Figure 7, where all ten wells were considered within the Pozo D-129 Formation. The pay lithofacies response corresponds to the lowest P-impedance and Vp/Vs (left) which is also associated with the highest effective porosity (right).

The petrophysical and rock physics model, which characterises the rock in terms of reservoir properties and elastic response, was consistent and played an essential role in the integration of geostatistical inversion and co-simulation.

In parallel, seismic conditioning was performed to increase the signal-to-noise ratio of the seismic data. This conditioning was first applied in the pre-stack domain and then in the post-stack domain. The post-stack conditioning is explained later in this article.

The processing steps applied to pre-stack CDP gathers were: Trim statics, radon de-multiple and COV de-noise. One gather example before and after conditioning is shown in Figure 8.

Pre-stack seismic conditioning produced high-quality data that was used as input for both deterministic and geostatistical inversions.

Deterministic AVA inversion, followed by probabilistic lithofacies classification, was also performed as part of the study but they are outside the scope of this article. The main benefit of deterministic inversion for the geostatistical inversion was its ability to quantify the signal-to-noise ratio for each seismic angle stack and across the study area.

Geostatistical inversion was the core component to achieve the goal of this study. This is a probabilistic method that integrates well logs, seismic and other geologic inputs to generate outcomes that honour all input data. Geostatistical inversion simultaneously generates several highly detailed equi-probable solutions (realisations) of elastic properties and lithofacies probabilities. These realisations exceed seismic vertical resolution. Additionally, by having several realisations it is possible to understand the range of uncertainty and associated geological risk. Several examples regarding the geostatistical inversion technique have been published in the literature which illustrate its benefits over deterministic methods, emphasising the importance of facies in the process and showing its successful application on synthetic and real data (Sams et al., 2011; Sams and Saussus, 2012; and Filippova et al., 2011).

Figure 9 illustrates the main differences between the results of the deterministic and geostatistical inversions. First, the deterministic inversion provides a prediction at seismic resolution, whereas the geostatistical inversion yields a much higher vertical resolution extracted from well data through a geostatistical model. Another difference is that the deterministic inversion generates a single 'optimum' solution while the geostatistical inversion produces several equi-probable solutions (20 realisations in this study). The number of realisations was chosen to obtain sensible statistics while balancing computing resources available and running times. This means that an uncertainty analysis can be performed based on the geostatistical inversion results but not on the deterministic inversion solution. A single realisation from the geostatistical inversion is shown in Figure 9. The third main difference comes from the match between the inversion result and measured well logs. The geostatistical inversion is constrained by the well data, which means that all realisations perfectly match the well logs. This is not the case for the deterministic inversion where variations from measured logs can be observed at the various well locations.

As shown in Figure 9, geostatistical inversion exceeds vertical seismic resolution which yields to successful characterisation of the thin reservoirs of Pozo D-129 Formation.

The final stage of the study was co-simulation of effective porosity. Co-simulation is a stochastic approach that generates several realisations of rock properties (effective porosity in this case) from geostatistical inversion. The co-simulation performed in this study used the relationship between P-impedance, Vp/Vs, density, and effective porosity from well logs to create Probability Density Functions (PDFs), as shown in Figure 10. The pay lithofacies is characterised by lower P-impedance, lower Vp/Vs, lower density, and higher effective porosity than the other two lithofacies (reservoir and non-reservoir). The pay lithofacies can be differentiated from the other two (reservoir and

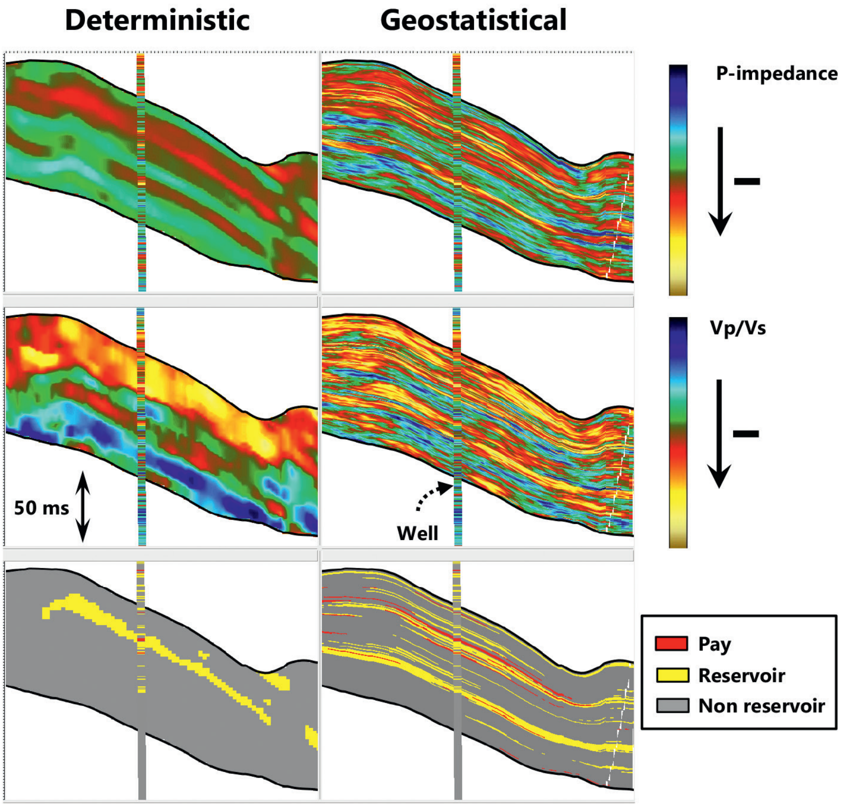

Figure 9 Comparison of a NW-SE profile extracted from the P-impedance, Vp/Vs, and lithofacies determined from (left) deterministic, and (right) geostatistical inversion. A single realisation out of the 20 computed for geostatistical inversion is shown.

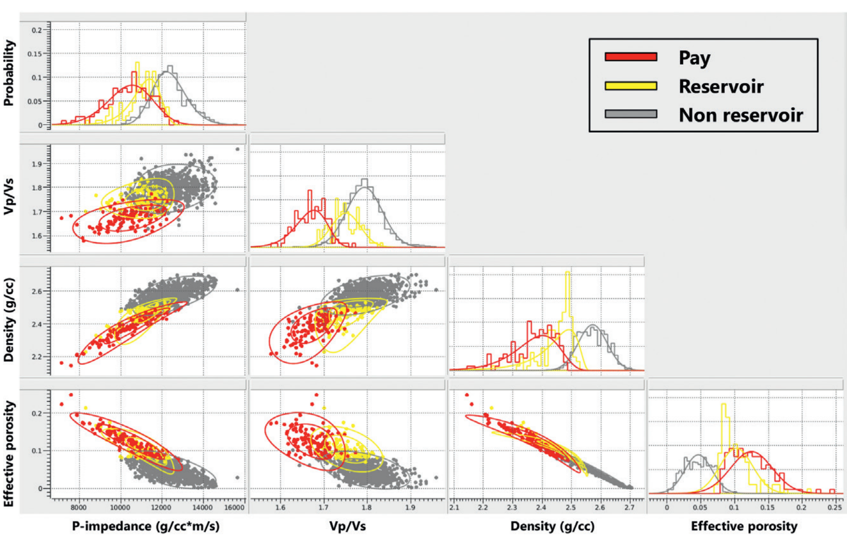

Figure 10 Crossplots between elastic properties and effective porosity exhibiting relationships, with the cluster points colour-coded with lithofacies. The PDFs are also included at the top of each column. The well log data plotted are from the petrophysics and rock physics model.

non-reservoir) even though some overlap between them is still present. In particular the Vp/Vs property seems to be the most effective discriminator.

Challenges

Several challenges had to be overcome during the course of this study. The first was the structurally complex fault systems which represented a real challenge for seismic imaging, seismic velocity and AVA compliance (the first two were not part of this case study). The most significant faults (15 in total) were incorporated into a stratigraphic/structural model used to support both the deterministic and geostatistical inversion (Figure 11).

The second challenge lay in the fact that seismic amplitudes were strongly unbalanced laterally and were not fully consistent across angles. To address this, amplitude normalisation was applied to the seismic angle stacks. This was achieved through computation of 3D scale factors for each angle stack independently. Figure 12 shows a section with the AVO gradient attribute computed from seismic angle stacks before and after post-stack conditioning. Before conditioning, a significant lateral variation in the energy of some reflectors can be observed. For instance, within the target interval highlighted by a red ellipse, the energy level appears dimmed compared to the areas on both sides. After conditioning, the AVO gradient energy is more balanced across the section. All in all, post-stack seismic conditioning improved the quality of the data used as input to the deterministic and geostatistical inversions.

The last challenge was the low seismic signal-to-noise ratio for some intervals as evidenced by a poor match in some well-to-seismic ties. Figure 13 shows the well-to-seismic tie displaying the AVO traces for one well in the Chulengo area. Correlation is variable both vertically and across angles (laterally). In this display two different intervals are highlighted. The blue rectangle highlights a relatively thick vertical window with very low seismic-synthetics cross-correlation (blue area). This window coincides with the Mina del Carmen Formation which was outside the scope of the geostatistical inversion even though it lies immediately above the target reservoirs of the Pozo D-129 Formation. The low cross-correlation in the Mina del Carmen Formation may be partly attributed to small impedance contrasts, resulting from the widespread presence of tuff throughout the interval. In contrast, the red rectangle shows an area where seismic-synthetics cross-correlation is high (yellow/orange colours) at this well location. The target reservoirs are located within this interval.

Also, some of the challenges faced during this study were related to seismic limitations. These limitations were attributed to several factors, including sparse acquisition survey geometries, aliased noise affecting near offset/angles, limited far offset/angles and significant topographic and weathering layer variability.

Finally, with the continuous advancement of seismic processing technologies, the current seismic dataset could benefit from the application of more advanced algorithms to further improve the seismic (and velocity field) quality and, as a result, the quality of the inversion products.

Results

Pay probability (posterior probability) is computed following Bayesian inference which is part of the geostatistical inversion method. Here, two approaches of 'prior' probability were compared: 1D versus 3D (Figure 14). In both cases, 140 vertical micro-layers were defined with an average thickness of 0.5 ms. As defined during the petrophysics analysis, three lithofacies were used: pay, reservoir and non-reservoir. The sum of each lithofacies probability equals 100%. As it can be observed in Figure 14, overall probabilities for non-reservoir lithofacies were by far higher than the other two, for both 1D and 3D approaches. Notably, the overall probabilities in the 1D approach were higher for pay than for the reservoir lithofacies, while in the 3D approach, the general probabilities were the lowest for pay lithofacies. This observation suggested that the general posterior pay probability might be lower with the 3D approach compared with the 1D approach.

To create the 3D prior probability models, we followed a three-step process. Firstly, we clustered available wells into three distinct areas: Chulengo (five wells), Koro (two wells), and a southwestern region outside the study area (two wells). Next, we computed 1D prior probabilities for each area and micro-layer using the available stratigraphic grid and litho-facies definitions at wells. We then defined three pseudo-wells, assigning each the corresponding 1D profiles, and located them at the midpoint of the wells in each area. Finally, we used the stratigraphic grid to interpolate the 1D prior probabilities of the pseudo wells for

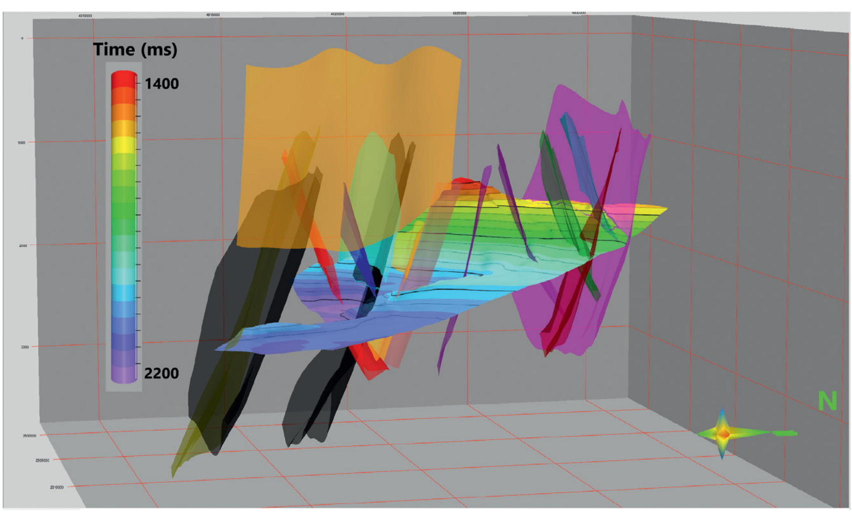

Figure 11 3D view illustrating the complex fault system within the study area: 15 faults are displayed along with the horizon for top of the Pozo-D129 Formation.

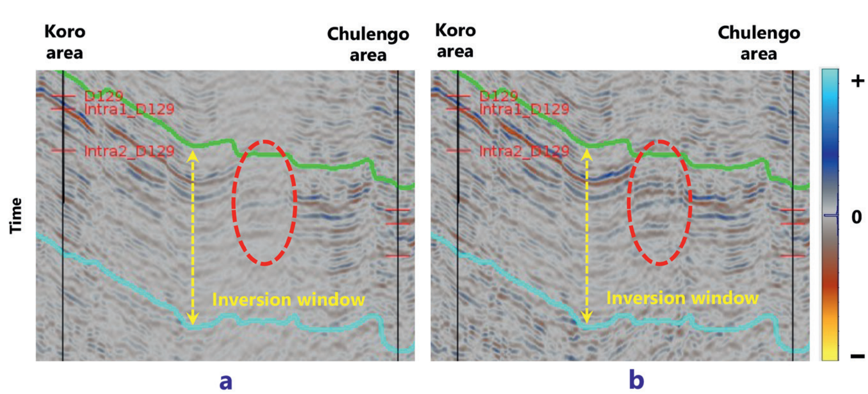

Figure 12 AVO gradient before (a) and after (b) post-stack conditioning. The red ellipse highlights an area where reflectors were enhanced after conditioning.

each litho-facies and micro-layer. Global kriging was employed as the interpolation method, with a variogram range of 50 km. Additionally, it is worth noting that the slope line interpreted from the separate attributes study was omitted in the construction of this model.

Pay probability maps following these two approaches are shown in Figure 15. By using the 1D approach, pay probability was overestimated according to fluid production data from a blind well located in the NW (Koro) area. On the other hand, the 3D approach produced a more realistic estimation of pay probability in general. This comparison also suggested that the 1D approach was simplistic to properly account for the lateral geological variations present in the study area.

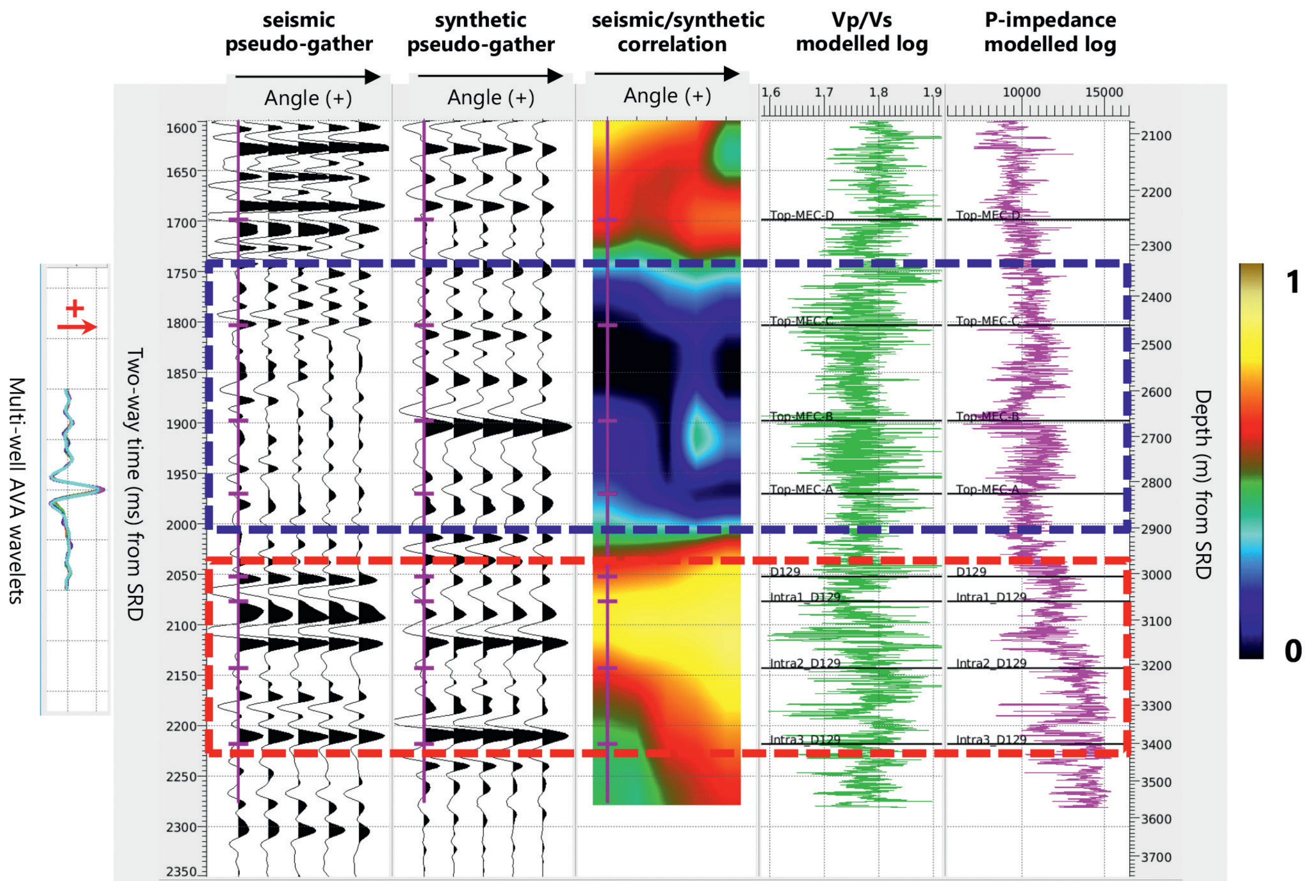

Figure 13 Well-to-seismic tie in AVO mode display in the Chulengo area.

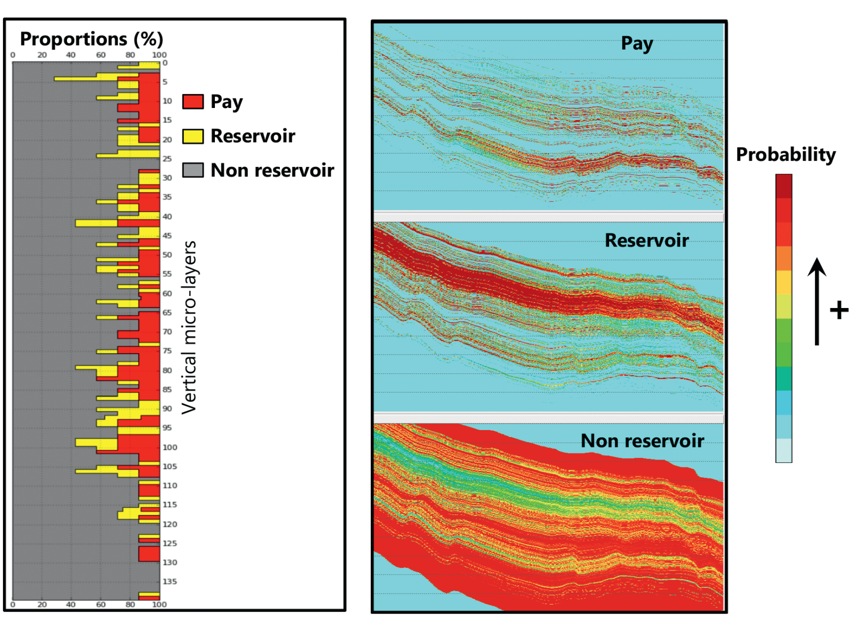

Figure 14 Prior probabilities: 1D (left) and 3D (right)

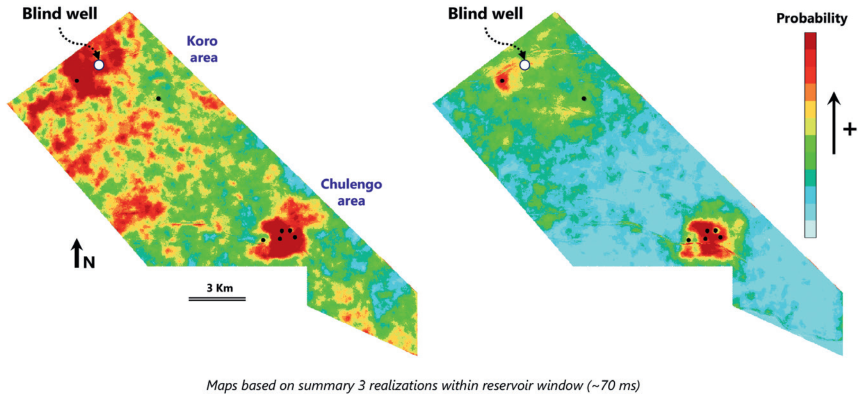

Figure 15 Pay probability maps from 1D (left) and 3D (right) prior probabilities.

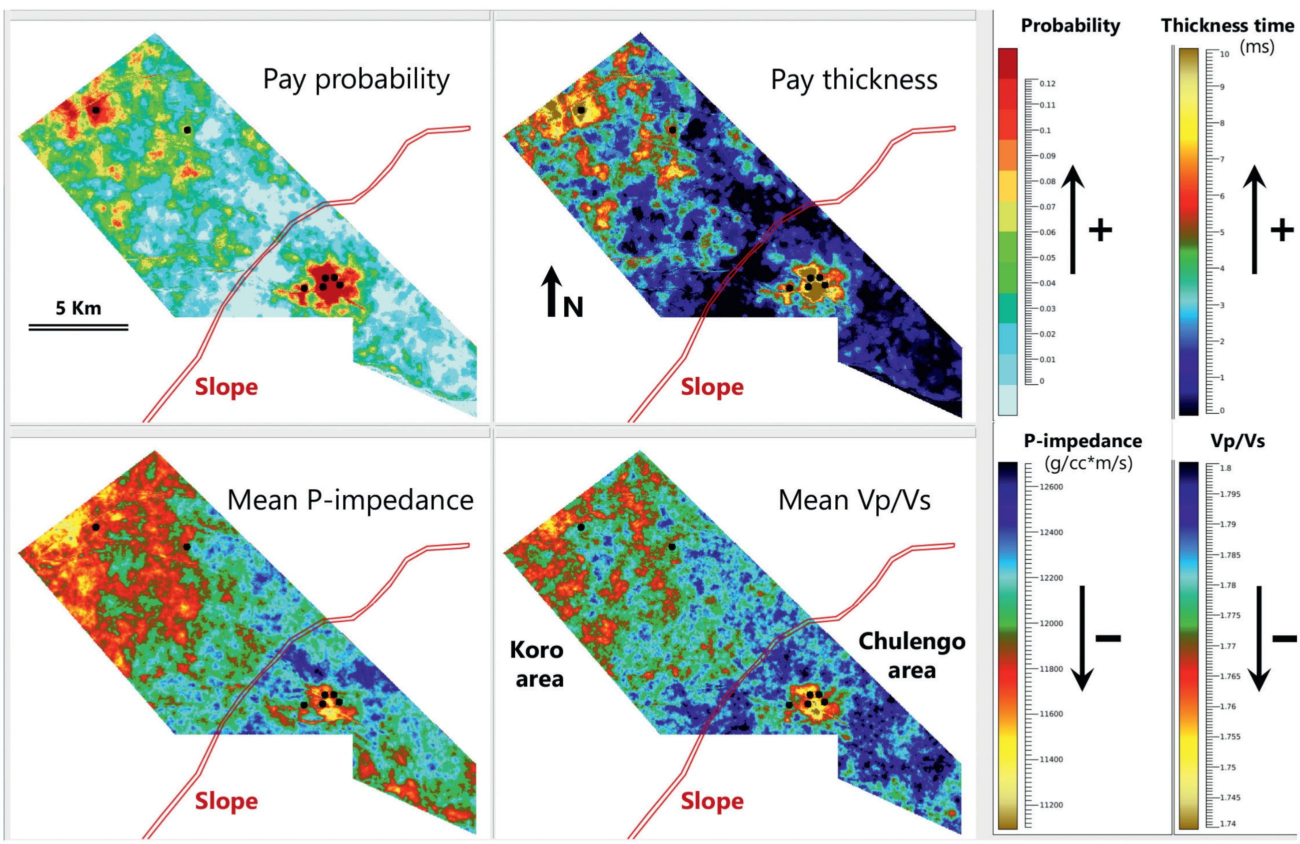

Figure 16 Maps within the reservoir window for realisation 20 and the slope line interpreted from seismic attributes as shown in Figure 4.

3D prior proportions for geostatistical inversion proved to be crucial for better characterisation of lithofacies between the Chulengo area (south-east) and the Koro area (north-west) compared with the 1D approach.

Final geostatistical inversion was generated by following the approach with 3D prior probabilities. One realisation is shown in Figure 16 along with the slope line interpreted from the separate seismic attributes study of the area. The slope line delimits the Koro area (NW) and the Chulengo area (SE). All maps show a level of consistency, in particular pay probability and pay thickness, showing similar lateral trends. Also, in Figure 16, it was observed that in general pay thickness and pay probability were consistently higher where P-impedance and Vp/Vs were lower.

When comparing the geostatistical inversion maps shown in Figure 16 with the conceptual depositional model (Figure 3) and the previous seismic attribute study (Figure 4) significant consistency was observed. This provided added confidence in the outcomes from the geostatistical inversion.

An arbitrary section through five producing wells (Chulengo area) showing part of the geostatistical inversion results and co-simulated effective porosity is shown in Figure 17. A single realisation is shown on the left-hand side and the most probable or average properties based on all 20 realisations are displayed on the right-hand side. As expected, the pay lithofacies correlates well with the highest effective porosity values. Additionally, the single realisation shows more details than the mean/most probable properties.

Figure 18 shows several average pay probability maps within the reservoir window around the location of five producing wells in the Chulengo area. The high probability zone delineates well this producing field. Also, lateral variations can be observed between the three random realisations. Statistical analysis of these differences made it possible to quantify the level of uncertainty (standard deviation, not shown in this article) associated with the pay probability.

Similarly, Figure 19 shows several average effective porosity maps covering the same area. The high effective porosity zone also delineates well this producing field. Again, lateral variations can be observed between the three random realisations, which were used to quantify the level of uncertainty (standard deviation, not shown in this article). Notably, it was also observed that the five wells of the Chu-

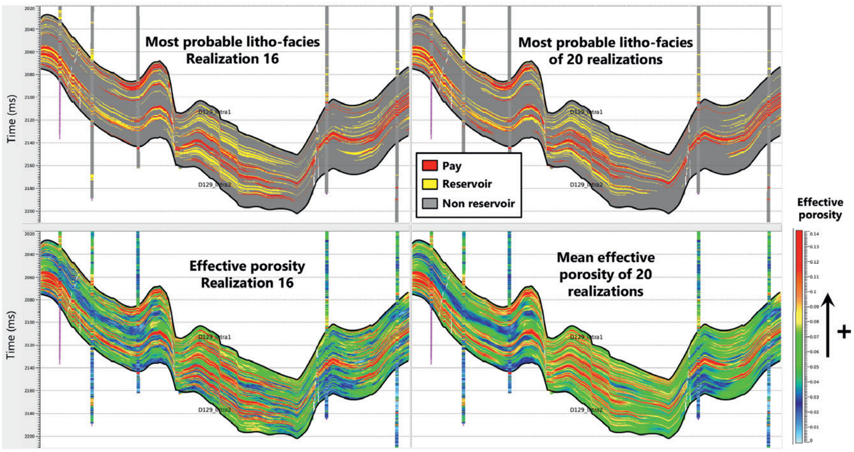

Figure 17 Arbitrary section through five producing wells in the Chulengo area showing part of the geostatistical inversion results and co-simulated effective porosity. A single realisation (left) and mean/most probable out of 20 realisations (right).

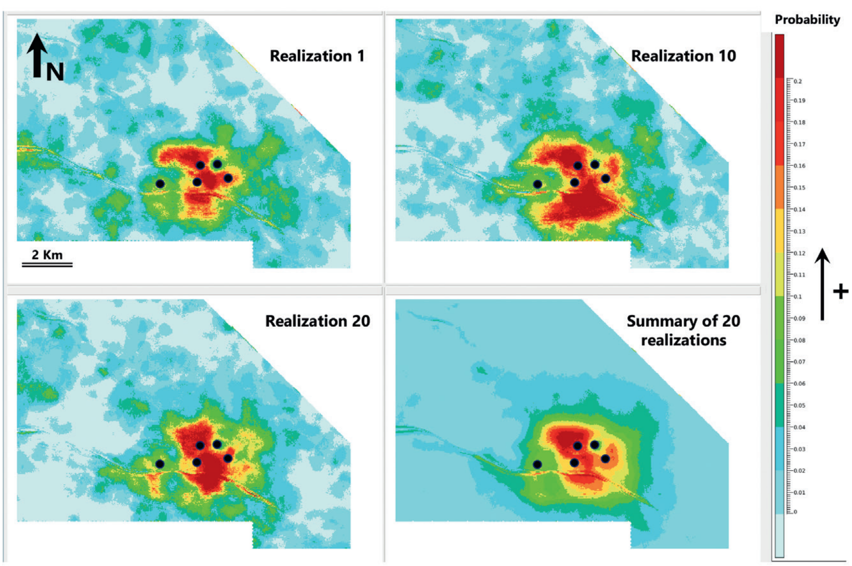

Figure 18 Average pay probability maps in the Chulengo area within the reservoir window (black dots correspond to five producing wells).

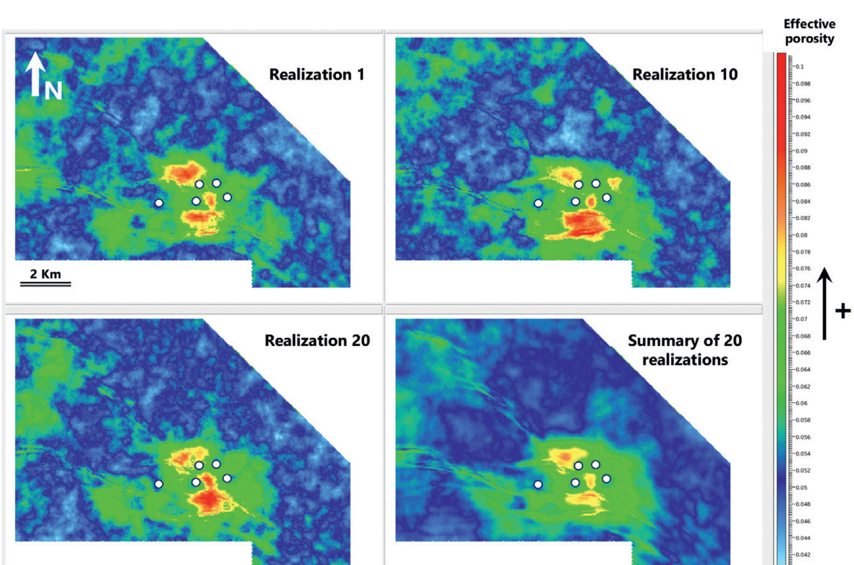

Figure 19 Average effective porosity maps in the Chulengo area within the reservoir window (white dots correspond to five producing wells).

lengo area were not located in zones with the highest effective porosity.

The lithofacies probability and effective porosity volumes will be used to build static models of the field that will allow estimation of the in-place gas volume along with its associated uncertainty. This data will be used to dynamically simulate the future development of this field.

Finally, regular interaction between the multi-disciplinary teams of Pan American Energy and Viridien was instrumental in ensuring the high quality of this integrated seismic reservoir characterisation study.

Conclusions

First, the primary objective of generating reliable input for building static models to conduct dynamic simulations of the Chulengo field has been successfully achieved through geostatistical inversion.

Second, the use of 3D prior probabilities for geostatistical inversion has proven crucial for better characterisation of litho-facies between the Chulengo area (south-east) and the Koro area (north-west), outperforming the 1D approach.

Third, the results of the geostatistical inversion, conceptual depositional model, and previous seismic attribute study, have shown significant consistency, increasing confidence in the outcomes of the geostatistical inversion.

Finally, the results of this study will be used to build static models of the field, enabling estimation of the in-place gas volume and its associated uncertainty. These models will also serve as input for dynamic simulations for the future development of this field.

Acknowledgements

We thank Juan Moirano and Lorena Caviglia from Pan American Energy and Andy Holman, Diego Lopez, Robert Porjesz and Fabien Allo from Viridien for insightful discussions and suggestions.

We thank Pan American Energy and Viridien for giving permission to publish this paper.

References

Brown, L.F., Jr. and Fisher, W.L. [1977]. Seismic-Stratigraphic Interpretation of Depositional Systems: Examples from Brazilian Rift and Pull-Apart Basins. In: Payton, C.E. (Ed.) *Seismic Stratigraphy – Applications to Hydrocarbon Exploration*, **26**, 213-248.

Canocini, A., Andersen, D. and Muniategui, M. [2023]. Metodología para caracterizar y desarrollar un yacimiento de gas exploratorio utilizando un modelo integrado de producción. Fm. D-129 en el Yacimiento Chulengo. Cerro Dragón. Cuenca del Golfo San Jorge. *8° Congreso de Producción y Desarrollo de Reservas*, Buenos Aires.

Cohen, M., Castillo, V., Fernandez, S., Galarza, B., García Torrejón, L., Millo, L., Plazibat, S., Poveda, L., Scasso, J. and Vernengo, L.F. [2022]. Exploración y Desarrollo de Hidrocarburos en Cerro Dragón, Cuenca del Golfo San Jorge, Argentina. Relatorio XXI, *Congreso Geológico Argentino, Geología y Recurso Naturales de la Provincia de Chubut*, 1463-1494, Puerto Madryn.

Filippova, K., Kozhenkov, A. and Alabushin, A. [2011]. Seismic inversion techniques: choice and benefits. *First Break,* **29**(5), 103–114. https://doi.org/10.3997/1365-2397.29.5.49948.

López Angriman, A., Zarpellón, C., Mussel, F. and Cohen, M. [2014]. Modelo Paleogeográfico de la sección Superior de la Formación Pozo D-129. Su aplicación al desarrollo de reservas en la cuenca del Golfo San Jorge, Argentina. *9° Congreso de Exploración y Desarrollo de Hidrocarburos,* Actas 1: 489-510, Mendoza.

Sams, M.S., Millar, I., Satriawan, W., Saussus, D. and Bhattacharyya, S. [2011]. Integration of geology and geophysics through geostatistical inversion: a case study. *First Break,* **29**(8), 47-56. https://doi.org/10.3997/1365-2397.2011023.

Sams, M.S. and Saussus, D. [2012]. Facies as the key to using seismic inversion for modelling reservoir properties. *First Break,* **30**(7), 45-52. https://doi.org/10.3997/1365-2397.2012009.

Zarpellón, C. [2010]. Modelo paleogeográfico de la sección superior de la Formación Pozo D-129: determinación del quiebre del talud mediante la utilización de atributos sísmicos. *Reporte interno Pan American Energy*. Unpublished report.